A new fluorescent hemicryptophane for acetylcholine recognition with an unusual recognition mode

Nicolas Fantozzi, Rémi Pétuya, Alberto Insuasty, Augustin Long, Sara Lefevre, Aline Schmitt, Vincent Robert, Jean-Pierre Dutasta, Isabelle Baraille, Laure Guy, et al.

A new fluorescent hemicryptophane for acetylcholine recognition with an unusual recognition mode

Nicolas Fantozzi,[a] Rémi Pétuya,[b] Alberto Insuasty,[c] Augustin Long,[c] Sara Lefevre,[d] Aline Schmitt,[d] Vincent Robert,[e] Jean-Pierre Dutasta,[d] Isabelle Baraille,[b] Laure Guy,[d] Emilie Genin,[a] Didier Bégué,[b] Alexandre Martinez,[c] Sandra Pinet*[a] and Isabelle Gosse*[a]

A new off–on fluorescent hemicryptophane probe for acetylcholine has been designed. This hemicryptophane, made fluorescent *via* an extension of the conjugation of its cyclotriveratrylene C_3-symmetry part, exhibits improved fluorescence properties compared with fluorescent hemicryptophanes previously described. Indeed, both the excitation and emission wavelengths are red-shifted and the quantum yield is increased. Moreover, this hemicryptophane is able to bind acetylcholine with a high association constant of 3.2×10^4 M^{-1}. This recognition process is accompanied by an increase in the brightness of the capsule. Surprisingly, contrary to what is commonly observed with cyclotriveratrylene-based hosts, the quaternary ammonium of the guest interacts with the tris(2-aminoethyl)amine south part of the hemicryptophane instead of the cyclotriveratrylene north part. This unusual binding mode is supported by both proton NMR experiments and density functional theory calculations.

Introduction

For both analytical sensing and optical imaging, luminescence is a technique of choice because of its high sensitivity, fast response time and technical simplicity.[1] In this context a plethora of luminescent sensors designed for the detection of metal ions[2] or anions[3] have been developed.[4] Biological relevant molecules[1,5] such as nucleotides,[6] reactive oxygen species[7] or neurotransmitters[8] have also attracted significant attention; their optical sensing remains a field of great interest. For instance, many optical nanomaterials such as quantum dots,[9] carbon dots,[10] nanodots,[11] nanoclusters[12] or nanoparticles[13] were used for the sensing of dopamine.[14] In many cases, the *o*-quinone resulting from the oxidation of the catecholamine is responsible for the signal quenching.

Fluorogenic molecules were also used for the detection of monoamines.[8a,15] In this case, the neurotransmitter acts as a reactant and forms, with the fluorogenic species, a new emissive product after reaction. However, the covalent binding of the neurotransmitter with the probe, may affect its behavior.

Among neurotransmitters, there is a particular interest in the detection of acetylcholine (ACh) because of its significant role in both the peripheral and central nervous systems. In particular, ACh role in learning and memory processes[16] and in locomotion has been identified.[17] Moreover, ACh is considered to be implicated in mood disorders[18] and neurodegenerative diseases.[19]

Because of its lack of fluorescent group or function that could be functionalized with a fluorogenic molecule, ACh's detection is difficult. Therefore, fluorometric biosensors based on H_2O_2-sensitive nanomaterials have been developed for ACh detection.[20] To be detected, the neurotransmitter has to be degraded in H_2O_2 first, which limits the use of such biosensors to the quantification of the target.

Supramolecular probes for the fluorescent detection of acetylcholine already exist.[21] In most cases, a low-fluorescent supramolecular system is used as the probe. This system consists of a fluorophore confined in the host molecule. In the presence of ACh, the dye is displaced and recovers its fluorescence. As for biosensors,

[a] *Université Bordeaux, CNRS, Bordeaux INP, Institut des Sciences Moléculaires, UMR 5255, F-33400, Talence, France. E-mail: sandra.pinet@u-bordeaux.fr, isabelle.gosse@u-bordeaux.fr*

[b] *Université de Pau et des Pays de l'Adour, E2S UPPA, CNRS, IPREM, Institut des Sciences Analytiques et de Physicochimie pour l'Environnement, UMR, 5254 Pau, France*

[c] *Aix Marseille Univ., CNRS, Centrale Marseille, iSm2, UMR 7113, 13397 Marseille, France*

[d] *Laboratoire de Chimie, École Normale Supérieure de Lyon, CNRS, UCBL, 46 allée d'Italie, F-69364 Lyon, France*

[e] *Laboratoire de Chimie Quantique, Institut de Chimie, UMR UDS-CNRS 7177, Université de Strasbourg, Institut Le Bel, 4 rue Blaise Pascal, F-67070 Strasbourg, France*

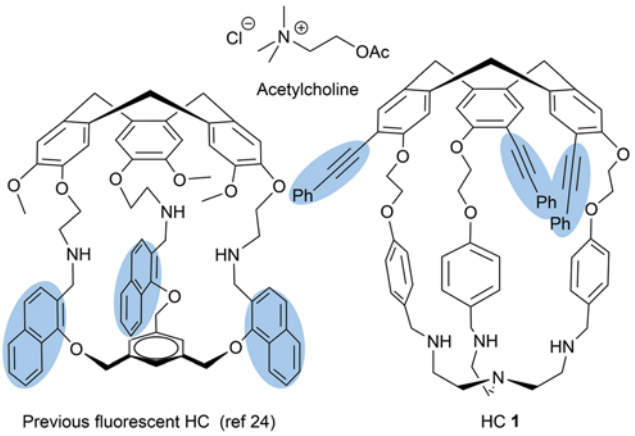

Fig. 1 Fluorescent hemicryptophane probes and targeted acetylcholine.

fluorescence variation measurements allow to quantify the ACh but not to perform its spatial and temporal monitoring. To enable imaging, the host molecule has to be fluorescent and its photochemical properties have to change during the recognition event, ideally leading to an enhancement of the emission intensity.

Fluorescent cyclotriveratrylenes (CTVs) able to recognize ammonium such ACh or choline has been elaborated in our group.[22] However, insufficient binding constants and selectivities were obtained. In order to circumvent these limitations we turned our investigation to molecular cages and more precisely hemicryptophanes (HCs), able to complex, among other guests, ammoniums in solution.[23] HCs are preorganized cavities made of a CTV unit and another C_3-symmetrical moiety, such as triamide, tris(2-aminoethyl)amine (TREN) or trialkanolamine groups. Tripodal benzenic platforms were also used. Very recently, we have described a fluorescent HC (Fig. 1, left) able to recognize ACh with a binding constant of 2.4×10^4 M^{-1} in a 98 : 2 DMSO : water mixture.[24] In the case of this HC, the fluorophore is integrated into the spacer connecting the two C_3-symmetrical units. In order to easily modulate independently both the cavity's size and the spectroscopic properties of HCs, we explored an alternative strategy consisting in grafting the fluorescent entity onto the CTV skeleton. Herein, we report on the synthesis, characterization and recognition properties of the new off–on fluorescent hemicryptophane probe **1** (Fig. 1). The fluorescence of HC **1** is due to the introduction of a π-conjugated group within the CTV unit; a TREN group was used as C_3-symmetrical moiety. Compared with the previous fluorescent HC, the capsule **1** allows for the quantification of ACh by both absorption and emission spectroscopies and a similar affinity constant for ACh was determined. Conversely to what is usually observed with CTVs or HCs, our results suggest that the ammonium part of ACh does not interact with the CTV moiety but with the C_3-symmetrical TREN unit. These observations are consistent with density functional theory (DFT) calculations.

Results and discussion

Synthesis of the hemicryptophane 1 and spectroscopic characterizations.

The hemicryptophane **1** was synthetized from 3-hydroxy-4-iodobenzoic acid **2** in six steps following the synthetic pathway described in Scheme 1. In DMF, 3-hydroxy-4-iodobenzoic acid was reacted with 1,2-dibromoethane in the presence of potassium carbonate to afford 3-(2-bromoethoxy)-4-iodobenzoate. This one was subsequently reduced in benzylic alcohol **3** using diisobutylaluminium hydride with a two-step overall yield of 68%. Then **3** was trimerized in the presence of phosphorus pentoxide to lead to the CTV **4** in 37% yield. Nucleophilic substitution of the bromine atoms by the phenoxides of 4-hydroxybenzaldehyde in DMF afforded **5** with 88% yield. This compound was transformed in **6** with 64% yield using ethynylbenzene in classical Sonogashira coupling conditions. Finally, reductive amination in the presence of tris(2-aminoethyl)amine drove to the desired hemicryptophane **1** in 20% yield after purification by column chromatography.

The proton NMR spectrum of **1** is consistent with the one expected for a compound with a C_3-symmetry (Fig. 2). The aromatic protons Ha and Hb of the CTV exhibit two singlets at 7.48 and 7.06 ppm respectively. Two typical doublets for the diastereotopic benzylic protons Hc and Hc′ of the CTV appear at 4.76 and 3.68 ppm respectively. The aromatic proton of the phenyl group, *i.e.* Hd, He and Hf, appear as two multiplets between 7.24 and 7.44 ppm. The two doublets at 6.78 and 6.62 ppm correspond to the aromatic protons of the phenoxy group (Hg and Hh) and the multiplets between 4.2 and 4.7 ppm to the diasterotopic protons of the ethylenglycol chain (Hi, Hi′, Hj and Hj′). The signals at 3.33 and

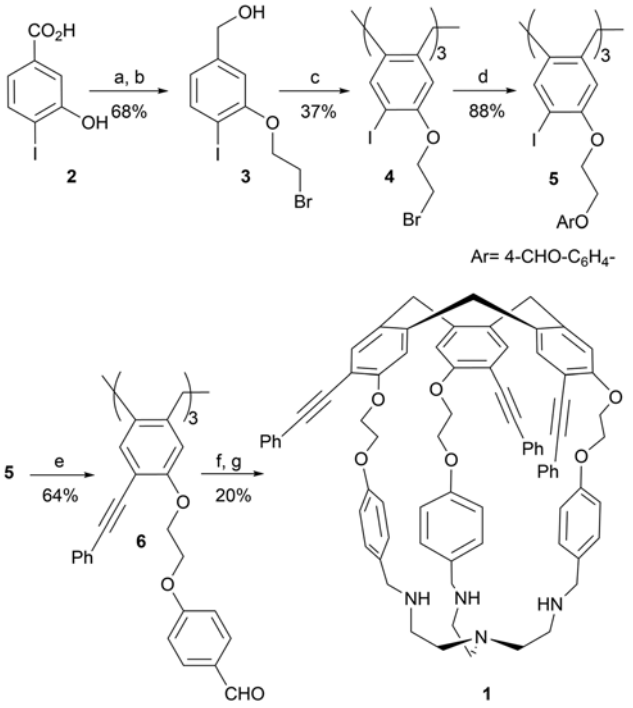

a) $BrCH_2CH_2Br$, K_2CO_3, DMF, 35°C, 16h; b) Dibal-H, THF, -80°C to r.t., 18h. c) P_2O_5, Et_2O, Δ, 4 d; d) p-hydroxybenzaldehyde, Cs_2CO_3, DMF, 40°C, 18h. e) Ethynylbenzene, $PdCl_2(PPh_3)_2$ (0.6 equiv.), CuI (0.6 equiv.), triethylamine, toluene, 40°C, N_2, 2 d; f) Tris(2-aminoethyl)amine, DMF/MeOH, 45°C, N_2, 3 d. g) $NaBH_4$, 0°C to 25°C, 4h.

Scheme 1 Access to the fluorescent hemicryptophane **1**.

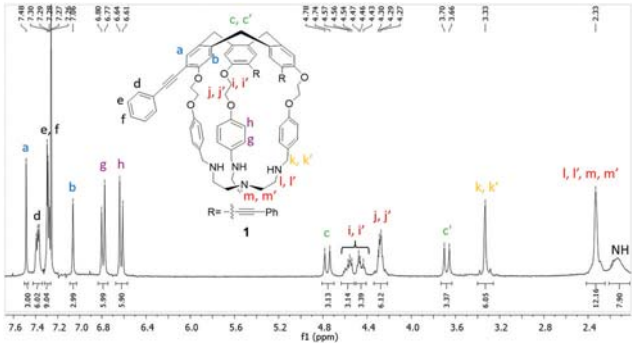

Fig. 2 ^{1}H NMR spectrum of HC **1** in $CDCl_3$ (300 MHz).

2.33 ppm are respectively assigned to the benzylic amine (Hk and Hk′) and the TREN fragment (Hl, Hl′, Hm and Hm′).

The absorption and emission properties of compound **1** were investigated in chloroform containing 2% of methanol (see Fig. S1 of ESI†). In such conditions, the HC **1** exhibits a maximum emission wavelength at 354 nm when excited at 319 nm ($\varepsilon = 8.33 \times 10^4\ M^{-1}\ cm^{-1}$). Absorption and emission spectra are very similar to the ones of the analogous CTV, in which the arms of the capsule were replaced by methyl groups.

Excited at 320 nm, this CTV exhibits a maximum emission at 355 nm.[25] This means that the structure of the capsule does not impact the spectroscopic characteristics of the fluorescent part. The fluorescent quantum yield Φ and the decay time τ were determined (Φ = 11% using quinine as reference and τ = 2.4 ns). Compared with the fluorescent HC previously described, the excitation and emission wavelengths are red-shifted and the quantum yield, that was inferior to 2%, is improved.[24]

Recognition properties of the hemicryptophane 1 for ACh

Having characterized the HC **1**, we investigated its binding properties toward ACh by absorption spectroscopy. Increased amounts of ACh were added to a 2.5×10^{-5} M solution of HC **2** in chloroform containing 2% of methanol. Upon addition an increase in the absorption intensity is observed but none isosbestic point (Fig. 3). As the ratio of the optical density of HC **1** in the presence of ACh to that in the absence of ACh (I/I_0) increases, linearly, upon successive additions of the quaternary ammonium (Fig. 3, inset), it is possible to use HC **1** to quantify the ACh amount by UV-visible spectroscopy.

This result encouraged us to study the ACh complexation by emission spectroscopy. Increasing amounts of ACh were added to a 2.5×10^{-5} M solution of HC **1** in chloroform containing 2% of methanol. Fig. 4 displays the spectrofluorometric titrations performed at 293 K. Upon addition of ACh, an enhancement of the emission intensity is observed. This enhancement is not linear. In fact, the quantum yield efficiency varies upon addition of ACh. It starts increasing to reach a maximum for six equivalents of ACh and then decreases linearly as ACh amount increases (Fig. 4, inset). As a consequence, the brightness enhancement is important at the beginning of the titration since it is correlated to an increase of both the absorption coefficient and the quantum yield. When the quantum yield efficiency starts decreasing, the brightness increases slower, until the increase of absorption coefficient is compensated

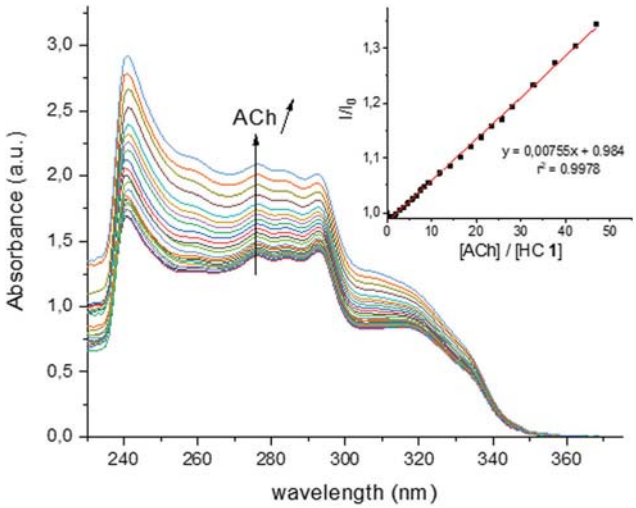

Fig. 3 Variation in HC **1** absorption spectra upon addition of ACh chloride, at 293 K in $CHCl_3$/MeOH (98/2). Inset: Linear increase of the HC **1** absorbance band at 319 nm with increasing amount of ACh chloride (0 to 50 equiv.).

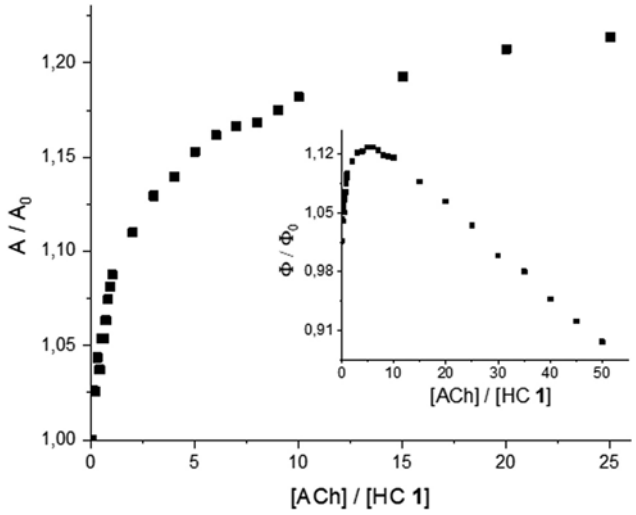

Fig. 4 Fluorescence emission area at 293 K of HC **1** (λ_{exc} = 319 nm) upon addition of ACh chloride in $CHCl_3$/MeOH (98/2). Inset: Quantum yield efficiency variation upon addition of ACh.

by the drop of the quantum yield efficiency. The drop of quantum yield efficiency is probably caused by the chloride anions used as counter ion of ACh and well-known to quench the emission of numerous fluorophores.[26]

The analysis of the titration curves shows the formation of a complex of stoichiometry 1 : 1 between ACh and the HC **1** (see ESI,† Fig. S2). The binding constant was determined using HypSpec® (Fig. S3 of ESI†). A high value of $3.2 \times 10^4\ M^{-1}$ has been found.

To confirm the complexation of ACh inside the HC **1** cavity and better address the involved interactions, we performed ^{1}H NMR titration experiments. To a solution of HC **1** in $CDCl_3$ were added aliquots of concentrated solutions of acetylcholine chloride (Fig. S4

and S5 of ESI†). In agreement with a fast host–guest exchange on the NMR time scale, the chemical shifts of the protons of both HC **1** and ACh vary when the ratio HC **1**/ACh varies. The signals of the methylene and methyl ammonium protons of the guest are shifted down-field when the ACh amount increases from 0.2 to 20 equivalents (Fig. S4, ESI†). In other words, compared to the spectrum of pure ACh, the signals of these protons are shifted up-field for a high amount of HC **1**, which is expected for the inclusion of a guest in an electron-rich host. Only the acetate signal is slightly shifted down-field for a high amount of host. Concerning the host, the signals of the north part's protons of the molecule are almost unaffected by the presence of ACh. On the other hand, the protons of the south part of the host molecule are shifted when the amount of the guest increases. More precisely, the signals of the benzylic protons (Hk and Hk′), of the phenoxy protons (Hg and Hh) and of the TREN protons (Hl, Hl′, Hm and Hm′) are all shifted downfield, the variation being much more important in case of protons Hg (Fig. S4 and S5, ESI†). These observations confirm the localization of ACh inside the electron rich HC cavity. Additionally, the downfield shifts observed for the south part's protons suggest these protons are close to a positive charge, in other word the ammonium function of the guest. This orientation of the ACh was not expected, as quaternary ammoniums, usually interact with the aromatic groups of the CTV part in complexes of ACh@CTV[22,27] and ACh@HC[24,28] in solution and also in solid state, as recently observed by Makita *et al.*[29] Nevertheless, these previous HCs able to complex ACh do not have a TREN as C_3-symmetry unit. It can be noticed that 1 : 2 host : guest stoichiometries have previously been observed for the complexation of chiral ammonium neurotransmitters by enantiopure hemicryptophane hosts bearing a TREN moiety.[30] The complexation of one ammonium by the CTV part and the interaction with the other ammonium guest with the TREN unit has been proposed to account for this result. This suggests that both the CTV and the TREN moieties of HCs are able to recognize the ammonium function.

Modelling of the interactions involved in the ACh@HC 1 complex by DFT calculations

To further confirm the formation of a ACh@HC **1** complex and rationalize the changes in the fluorescence response of the system in the presence or absence of ACh, host–guest interactions were modelled *via* DFT calculations (see Experimental section for details). Geometry optimizations were performed for both the hemicryptophane with ACh guest and the empty cage (Fig. 5). Two possible orientations of the acetylcholine were probed, with the ammonium pointing towards the CTV moiety or opposite to it, towards the TREN sub-unit (Fig. S6–S9 of ESI†). According to our calculations, the configuration with the ammonium pointing towards the TREN part is favoured by about 20 kcal mol^{-1}. In this configuration, hydrogen bonds exist between the nitrogen atoms of the TREN and both the methylene and methyl protons of the quaternary ammonium for which distances varying from 2.2 and 3.1 Å were determined.[31] Thus the TREN moiety probably plays a role in the recognition mode. Additionally, two hydrogen bonds exist also (i) between the oxygen carbonyl atom of the ACh and one hydrogen atom of the ethylenedioxy chain (2.4 Å) on one side of the guest and

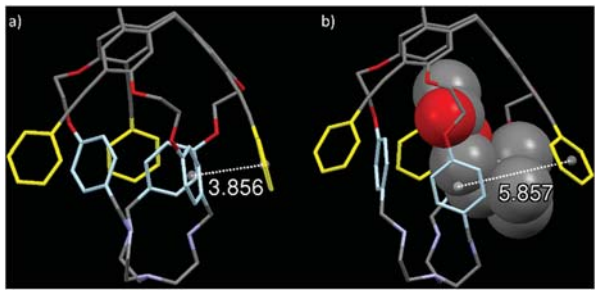

Fig. 5 Capped stick model of the DFT structures of hemicryptophane **1** optimized (a) without and (b) with acetylcholine. Colors are used to help differentiate the aromatic rings of alkynylbenzene units (in yellow) from those from HC arms (in light blue). For clarity purpose, hydrogen atoms are not represented and ACh guest is represented in "spacefill" style in which the atoms size corresponds to their van der Waals radius.

(ii) between an oxygen of an ethylenedioxy and an hydrogen of a methyl from the quaternary ammonium (2.4 Å) on the opposite side. The hydrogen bond involving the oxygen atom of the carbonyl group may explain the slight down-field shift observed for the methyl acetate signal during the ^{1}H NMR titration experiment. Finally, distances between 4.1 and 4.9 Å were measured between the ammonium nitrogen of the guest and the centers of the phenoxy rings. These distances correspond to close π–cation interactions.[32] As phenoxy aryl groups are electron rich, this is coherent with the observed up-field shift of the ammonium protons in NMR experiment. Thus, modelling results agree with the proton NMR complexation study according to which the ACh ammonium part is orientate towards the TREN moiety. The extended conjugation of the CTV moiety probably alters the electron density in the vicinity of its aromatic rings, leading to preferential cation–π interactions with the phenoxy group of the linker instead of the aromatic rings of the CTV unit, which might also account for the unusual complexation of ACh. All these measures are displayed in detail in the ESI† (Fig. S10–S12).

In the absence of ACh guest, π–π interactions are observed between the aromatic rings of the alkynylbenzene parts (in yellow) and the aromatic rings of the hemicryptophane arms (in light blue) with an average distance between these aromatic groups of 3.8 Å (see Fig. S6 and S7 of ESI†). When ACh is added, both type of aromatic centers rearrange to accommodate the guest molecule. The π–π interaction on the right side of the system (Fig. 5), highlighted by centroid to centroid distance measurement is a particularly striking example. The alkynylbenzene displayed on the right moves apart and is separated from its interacting aromatic from the HC which moves and rotates. Consequently, the distance between these aromatic centers increases from 3.9 Å to 5.9 Å. Fig. S8, given in the ESI,† displays overlays of the cages when modelled empty (in light blue) and filled (in orange) which highlights the structural changes around the aromatic centers. Overall, the swelling of the cage filled with ACh induces a significant decrease of two of the three π–π interactions (see Fig. S6 and S7, ESI†), thus limiting the non-radiative deexcitation processes and leading to an increase of the quantum fluorescence efficiency.

Experimental section

Chemicals and materials

All commercially available reagents were of commercial grade and used as received unless specified. 3-Hydroxy-4-iodobenzoic acid, dibromoethane, tris(2-aminoethyl)amine, trimethylamine, diisobutylaluminium hydride, sodium borohydride, phosphorus pentoxide, copper iodide, cesium carbonate and anhydrous DMF were purchased from Sigma Aldrich. Phenylacetylene, 4-hydroxybenzaldehyde, and bis(triphenylphosphine)palladium(II) dichloride were purchased from Acros, Alfa Aesar and fluorochem respectively. All other solvents were purchased from VWR. Methanol and triethylamine were dried over calcium hydride and freshly distilled under inert atmosphere before used. Toluene was distilled from sodium benzophenone ketyl under nitrogen atmosphere. THF, ether and dichloromethane were dried over activated alumina columns on Inert Solvent Purification System (SPS) under argon flush. Anhydrous *N*,*N*-dimethylformamide was kept under argon atmosphere.

Thin layer chromatography was carried out with Merck silica gel 60 F254 plates.

Column chromatography was performed using VWR 40–63 μm silica gel.

Melting points were determined with a Stuart scientific melting point apparatus SMP3 and are uncorrected.

IR spectra were recorded on a Nicolet iS10 FT-IR spectrometer.

HRMS (ESI-MS) were performed on various mass spectrometers. A Waters SYNAPT G2 HDMS mass spectrometer with an atmospheric pressure ionization (API) source was used for the mass spectra of compounds **3**, **4** and **5**. Agilent 6560 mass spectrometer was used in case of compounds **1**. Spectra were obtained with TOF analysis. A Q Exactive Hybrid Quadrupole-Orbitrap mass spectrometer was used for the analysis of **6**.

NMR spectra were recorded on either a Bruker Avance 300 or a Bruker Avance 600 spectrometer. Chemical shifts are reported using the residual solvent peak as internal reference for ^{1}H or for ^{13}C.

Steady-state absorption spectra were recorded between 200 nm and 500 nm on a Varian Cary 100 Scan spectrophotometer, using a quartz cuvette (1 cm × 1 cm × 4.5 cm).

Photoluminescence spectra were collected with a Varian Eclipse fluorescence spectrophotometer. The emission spectrum (λ_{exc} = 319 nm) was recorded between 328 nm and 450 nm with a maximum at 354 nm. All the emission spectra were corrected. Emission quantum yield was determined by using quinine sulfate as reference standard, which has a known emission quantum yield of 0.65 in 0.5 M sulfuric acid.[33] The reported fluorescence quantum yield is within ±10%. In the titration experiments guest aliquots were added with a microsyringe to a 2×10^{-5} M solution of **1** in chloroform containing 2% of methanol, placed in the fluorimeter cell at 20 °C. After each guest addition, the cell was stirred for 2 min before recording the emission spectrum. Integrated signals rather than peak heights were used in the titrations. The volume change due to the additions is taken into account in the calculation. 3 experiments were performed to verify their reproducibility.

Photoluminescence emission (A/A_0), based on the titration data, represents the PL emission area of the probe in the presence of the guest (A) normalized to the initial PL emission area (A_0) in the absence of the anion. Time-resolved fluorescence measurements were performed on dilute solutions (*ca.* 10^{-6} M, optical density 0.1) in standard 1 cm quartz cuvettes using an Edinburgh Instruments (FLS920) spectrofluorimeter in photon-counting mode. Fluorescence lifetimes were measured by time-correlated single-photon counting (TCSPC) using the same FLS920 spectrofluorimeter. Excitation was achieved by a hydrogen-filled nanosecond flash lamp (repetition rate 40 kHz). The instrument response (FWHM *ca.* 1 ns) was determined by measuring the light scattered by a Ludox suspension.

For the determination of formation constants, the spectrophotometric data were fitted with the program HypSpec®.[34]

Synthesis of various compounds

3-(2-Bromoethoxy)-4-iodobenzyl alcohol 3. To a solution of 3-hydroxy-4-iodobenzoic acid **2** (4 g, 15.15 mmol) in anhydrous DMF (220 mL) under nitrogen atmosphere were added K_2CO_3 (8 g, 60.6 mmol, 4 eq.) and dibromoethane (11.5 mL, 151.5 mmol, 10 eq.). The mixture was stirred and heated at 35 °C for 16 h. The solvent was removed under vacuum and the residue dissolved in diethyl ether (100 mL) and distilled water (100 mL). The layers were separated. The aqueous phase was extracted with Et_2O (2 × 100 mL). The combined organic layers were washed with water until neutrality, dried over anhydrous Na_2SO_4 filtered and concentrated under vacuum. The crude solid was purified by silica gel column chromatography using a (92/8) cyclohexane/AcOEt mixture as eluent. The solvent was then evaporated to give 2-bromoethyl 3-(2-bromoethoxy)-4-iodobenzoate as a white solid (5 g). This one was dissolved in anhydrous THF (60 mL), under inert atmosphere. To the resulting solution was added dropwise, at −80 °C, a solution of DIBAL-H (1 M in THF, 42 mL, 42 mmol). At the end of the addition, the solution was allowed to warm at room temperature and was stirred at 25 °C for 18 h. The mixture was cooled down to 0 °C before quenching the reaction with 1 M HCl (50 mL). The aqueous phase was extracted with DCM (3 × 100 mL). The combined organic layers were washed with distilled water until neutrality, dried over anhydrous sodium sulfate and concentrated under vacuum. The crude was purified by silica gel column chromatography using a (75/25) cyclohexane/AcOEt as eluent to give 3-(2-bromoethoxy)-4-iodobenzyl alcohol **3** as a white solid (3.67 g, 68%). R_f = 0.30 (cyclohexane/AcOEt 3/1); mp 60 °C; FTIR (neat) ν_{max}/cm^{-1} 3313 and 3226 (OH), 3091, 3066 and 3032 (CH_{Ar}), 2923 and 2866 (CH_2), 1585, 1573 and 1476 (C═C), 1451 (CH_2), 1255 (C–O), 575 (CBr); ^{1}H NMR δ_H (400 MHz, $CDCl_3$) 7.73 (1H, d, $^{3}J_{H,H}$ = 8.0 Hz, Ar-H), 6.84 (1H, s, Ar-H), 6.71 (1H, d, $^{3}J_{H,H}$ = 8.0 Hz, Ar-H), 4.63 (2H, d, $^{3}J_{H,OH}$ = 3.5 Hz, CH_2-Ar), 4.33 (2H, t, $^{3}J_{H,H}$ = 6.4 Hz, CH_2O), 3.68 (2H, t, $^{3}J_{H,H}$ = 6.4 Hz, CH_2Br), 1.91 (1H, br t, $^{3}J_{H,OH}$ = 3.5 Hz, OH); ^{13}C NMR δ_C (100 MHz, $CDCl_3$) 156.96 (C_{Ar}–O), 142.94 (C_{Ar}-CH_2OH), 139.55 (CH_{Ar}), 121.51 (CH_{Ar}), 111.10 (CH_{Ar}), 85.33 (C_{Ar}–I), 69.14 (C_{Ar}-CH_2O), 64.51 (CH_2O), 28.56 (CH_2Br); HRMS (ESI-TOF): m/z calcd for $C_9H_{10}O_2BrI + NH_4^+$: 373.9247 $[M + NH_4]^+$; found: 373.9247.

Synthesis of compound 4

A suspension of phosphorus pentoxide (1.97 g, 13.88 mmol, 3.3 eq.) in anhydrous diethyl ether (4 mL) was added, under nitrogen atmosphere, to a stirred solution of 3-(2-bromoethoxy)-4-iodobenzyl

alcohol **3** (1.5 g, 4.2 mmol) in dried diethyl ether (21 mL). The mixture was heated to reflux under vigorous stirring until the mixture forms a mass. Then, the stirring was stopped but the reflux was maintained for two days. More phosphorus pentoxide (0.68 g, 4.79 mmol, 1.14 eq.) was added to the reaction mixture and this one was heated to reflux for another two days. The solvent was removed under vacuum. The resulting dark residue was triturated with dichloromethane and filtered through silica gel in a large, fritted glass funnel. The silica gel was rinsed with dichloromethane. The mother liquor was concentrated to give the CTV **4** as a white solid (530 mg, 37%). mp 280 °C (decomposition); FTIR (neat) ν_{max}/cm^{-1} 3017 and 3010 (CH_{Ar}), 2975, 2963, 2911, 2863 and 2836 (CH_2), 1584 and 1483 (C═C), 1450 (CH_2), 1255 (C–O), 577 (CBr); ^{1}H NMR δ_H (600 MHz, DMSO) 7.99 (3H, s, Ar-H), 7.19 (3H, s, Ar-H), 4.67 (3H, d, $^2J_{H,H}$ = 13.4 Hz, Ar-CH_2), 4.39 (3H, ddd, $^2J_{H,H}$ = 11.3, $^3J_{H,H}$ = 5.9, 5.5 Hz, OC*H*$_2$CH$_2$Br), 4.33 (3H, ddd, $^2J_{H,H}$ = 11.3, $^3J_{H,H}$ = 5.8, 5.4 Hz, OC*H*$_2$CH$_2$Br), 3.78 (6H, 2dd, $^3J_{H,H}$ = 5.9, 5.8, 5.5, 5.4 Hz, OCH$_2$C*H*$_2$Br), 3.61 (3H, d, $^2J_{H,H}$ = 13.4 Hz, Ar-CH_2); ^{13}C NMR δ_C (150 MHz, DMSO) 155.13(3C, C_{Ar}–O), 141.50 (3C, $C_{Ar}CH_2$), 140.17 (3C, CH_{Ar}), 134.28 (3C, $C_{Ar}CH_2$), 114.31 (3C, CH_{Ar}), 84.58 (3C, C_{Ar}–I), 69.06 (3C, CH_2O), 34.24 (3C, Ar*C*H$_2$), 30.91 (3C, CH_2Br); HRMS (ESI-TOF): *m*/*z* calcd for $C_{27}H_{24}Br_3I_3O_3 + NH_4^+$: 1035.6711 $[M + NH_4]^+$; found: 1035.6700.

Synthesis of compound 5

A mixture of compound **4** (530 mg, 0.521 mmol), Cs_2CO_3 (746 mg, 2.288 mmol, 4.4 eq.) and *p*-hydroxybenzaldehyde (210 mg, 1.716 mmol, 3.3 eq.) in DMF (9 mL) was stirred at 40 °C for 18 h. The solvent was removed under vacuum. The resulting solid was washed with ethyl acetate, with a 10% aqueous sodium hydroxide solution and finally with water. The resulting product was dried under vacuum to lead to a white solid, the compound **5** (520 mg, 88%). mp 160 °C (decomposition); FTIR (neat) ν_{max}/cm^{-1} 3097, 3073, 3040 and 3027 (CH_{Ar}), 2921, 2871 and 2834 (CH_2), 2796 and 2737 (CHO), 1676 (CO), 1597, 1575, 1505 and 1477 (C═C), 1448 (CH_2), 1252 (C–O); ^{1}H NMR δ_H (600 MHz, DMSO) 9.86 (3H, s, CHO), 8.01 (3H, s, Ar-H), 7.85 (6H, d, $^3J_{H,H}$ = 8.8 Hz, Ar-H), 7.25 (3H, s, Ar-H), 7.16 (6H, d, $^3J_{H,H}$ = 8.8 Hz, Ar-H), 4.70 (3H, d, $^2J_{H,H}$ = 13.3 Hz, Ar-CH_2), 4.50–4.40 (9H, m, OCH_2), 4.39–4.32 (3H, m, OCH_2), 3.63 (3H, d, $^2J_{H,H}$ = 13.3 Hz, Ar-CH_2); ^{13}C NMR δ_C (150 MHz, DMSO) 191.31 (3C, CHO), 163.28 (3C, C_{Ar}–O), 155.56 (3C, C_{Ar}–O), 141.54 (3C, C_{Ar}-CH_2), 140.13 (3C, CH_{Ar}), 134.17 (3C, C_{Ar}-CH_2), 131.83 (6C, CH_{Ar}), 129.80 (3C, C_{Ar}-CHO), 115.13 (6C, CH_{Ar}), 114.32 (3C, CH_{Ar}), 84.66 (3C, C_{Ar}–I), 67.72 (3C, CH_2O), 66.66 (3C, CH_2O), 34.37 (3C, Ar*C*H$_2$); HRMS (ESI-TOF) *m*/*z* calcd for $C_{48}H_{39}I_3O_9 + NH_4^+$: 1158.0067 $[M + NH_4]^+$; found: 1158.0067.

Synthesis of compound 6

Compound **5** (200 mg, 0.175 mmol), phenylacetylene (162 mg, 1.58 mmol, 9 eq.), copper iodide (20 mg, 0.105 mmol, 0.6 eq.) and bis(triphenylphosphine)palladium(II) dichloride (70 mg, 0.1 mmol) were added in a dried-bottom flask. Distilled toluene (5.2 mL) was added under nitrogen atmosphere followed by anhydrous triethylamine (1.28 mL, 9.18 mmol) and the mixture was stirred at 40 °C for two days. The reaction mixture was cooled to room temperature before being concentrated under vacuum. The crude product was first purified by column chromatography on silica gel using an eluent gradient (CH_2Cl_2 to CH_2Cl_2/EtOAc 1/1). The resulting solid was dissolved in chloroform and precipitated by addition of diethyl ether. After filtration **6** was obtained pure (120 mg, 64%). R_f = 0.3 (DCM/AcOEt 97/3); mp 170 °C (from $CHCl_3$–Et_2O, decomposition); FTIR (neat) ν_{max}/cm^{-1} 3063 and 3030 (CH_{Ar}), 2920, 2876 and 2822 (CH_2), 2796 and 2734 (CHO), 2211 (CC), 1682 (CO), 1597, 1575, 1501 and 1480 (C═C), 1447 (CH_2), 1239 (C–O); ^{1}H NMR δ_H (600 MHz, $CDCl_3$) 9.76 (3H, s, CHO), 7.66 (6H, d, $^3J_{H,H}$ = 8.6 Hz, Ar-H), 7.42 (3H, s, Ar-H), 7.39 (6H, dd, $^3J_{H,H}$ = 8.1, $^4J_{H,H}$ = 1.4 Hz, Ph), 7.27 (3H, tt, $^3J_{H,H}$ = 7.5, $^4J_{H,H}$ = 1.4 Hz, Ph), 7.22 (6H, dd, $^3J_{H,H}$ = 8.1, 7.5 Hz, Ph), 6.94 (6H, d, $^3J_{H,H}$ = 8.6 Hz, Ar-H), 6.87 (3H, s, Ar-H), 4.49–4.25 (15H, 3m, Ar-CH_2 + CH_2O), 3.47 (3H, d, $^2J_{H,H}$ = 13.4 Hz, Ar-CH_2); ^{13}C NMR δ_C (150 MHz, $CDCl_3$) 190.67 (3C, CHO), 163.62 (3C, C_{Ar}–O), 157.94 (3C, C_{Ar}–O), 141.33 (3C, C_{Ar}-CH_2), 134.50 (3C, CH_{Ar}), 131.90 (3C, C_{Ar}-CH_2), 131.70 (6C, CH_{Ar}), 131.44 (6C, CH_{Ph}), 130.11 (3C, C_{Ar}-CC-Ph), 128.35 (6C, CH_{Ph}), 128.28 (3C, CH_{Ph}), 123.37 (3C, C_{Ph}-CC), 114.93 (6C, CH_{Ar}), 114.58 (3C, C_{Ar}-CHO), 112.25 (3C, CH_{Ar}), 93.61 (3C, Ph-*C*C-Ar), 85.62 (3C, Ph-C*C*-Ar), 67.67 (3C, CH_2O), 66.95 (3C, CH_2O), 36.35 (3C, Ar*C*H$_2$); HRMS (ESI) *m*/*z* calcd for $C_{72}H_{54}O_9 + Na^+$: 1085.36600 $[M + Na]^+$; found: 1085.36366.

Synthesis of hemicryptophane 1

To a stirred solution of **6** (120 mg, 113 μmol) in a mixture of dried DMF/MeOH 9/1 (100 mL) under nitrogen was added dropwise a solution of tris(2-aminoethyl)amine (19 μL, 126 μmol, 1.1 eq.) dissolved in the same solvent mixture (40 mL). The solution was heated to 45 °C for 3 days. The temperature was cooled to 0 °C before adding sodium borohydride (111 mg, 2.9 mmol, 25 eq.) to the solution. At the end of the addition, the mixture was allowed to warm at 25 °C and was stirred at this temperature for 4 hours. After concentration of the mixture under vacuum, the recovered residue was dissolved in chloroform (50 mL). A 10% aqueous solution of sodium hydroxide (20 mL) was added. The organic layer was separated and the aqueous phase extracted with chloroform (2 × 50 mL). The combined organic layers were washed with 10% aqueous NaOH (2 × 50 mL), dried over anhydrous sodium sulfate and concentrated under vacuum. The solid was purified by column chromatography on silica gel (eluent: $CHCl_3$/MeOH/Et_3N 90 : 10 : 2). The product was then washed several times with diethyl ether to give **1** (27 mg, 20%) as a white powder. R_f = 0.10 ($CHCl_3$/MeOH/Et_3N 90/10/2); mp 120 °C (decomposition); UV absorption: λ_{max} ($CHCl_3$/MeOH 98/2)/nm 241, 260, 276, 284, 293, 319 and 334 (ε/dm^3 mol^{-1} cm^{-1}) 167 900, 130 200, 141 700, 139 700, 144 800, 83 300 and 47 000); fluorescence emission: λ_{em} ($CHCl_3$/MeOH 98/2)/nm 354 (λ_{ex} = 319 nm; Φ = 11% (quinine as reference); FTIR (neat) $\nu = \nu_{max}$/cm^{-1} 3388 and 3309 (NH), 3054 and 3030 (CH_{Ar}), 2920, 2868, 2843 and 2815 (CH_2), 2210 (CC), 1606, 1592, 1506 and 1485 (C═C), 1452 (CH_2), 1242 (C–O); ^{1}H NMR δ_H (300 MHz, $CDCl_3$) 7.48 (3H, s, Ar-H), 7.38 (6H, dd, $^3J_{H,H}$ = 7.5, $^4J_{H,H}$ = 3.8 Hz, Ph), 7.32–7.26 (9H, m, Ph), 7.06 (3H, s, Ar-H), 6.79 (6H, d, $^2J_{H,H}$ = 8.6 Hz, Ar-H), 6.63 (6H, d, $^2J_{H,H}$ = 8.6 Hz, Ar-H), 4.76 (3H, d, $^2J_{H,H}$ = 13.6 Hz, Ar-CH_2), 4.56 (3H, ddd, $^2J_{H,H}$ = 12.3, $^3J_{H,H}$ = 5.7, 4.3 Hz, OCH_2), 4.46 (3H, ddd, $^2J_{H,H}$ = 12.3, $^3J_{H,H}$ = 4.1, 3.8 Hz, OCH_2), 4.34–4.20 (6H, m, OCH_2), 3.68 (3H, d, $^2J_{H,H}$ = 13.6 Hz, Ar-CH_2),

3.40–3.25 (6H, m, Ar-CH_2N), 2.41–2.23 (12H, m, CH_2N), 2.13 (3H, br s, NH + water); ^{13}C NMR δ_C (150 MHz, $CDCl_3$) 158.04 (3C, C_{Ar}–O), 157.52 (3C, C_{Ar}–O), 141.12 (3C, C_{Ar}-CH_2), 134.58 (3C, CH_{Ar}), 131.91 and 131.55 (12C, C_{Ar}-CH_2 + CH_{Ph} + $C_{Ar}CH_2$N), 129.27 (6C, CH_{Ar}), 128.20 (6C, CH_{Ph}), 128.05 (3C, CH_{Ph}), 123.58 (3C, C_{Ph}-CC-Ph), 116.12 (3C, CH_{Ar}), 114.92 (6C, CH_{Ar}), 112.81 (3C, C_{Ar}-CC-Ph), 93.20 (3C, Ph-*C*C-Ar), 85.79 (3C, Ph-C*C*-Ar), 68.50 (3C, CH_2O), 67.19 (3C, CH_2O), 52.68 (3C, Ar-*C*H_2N), 46.46 (6C, N*C*H_2*C*H_2N), 36.48 (3C, Ar*C*H_2); HRMS (ESI) *m*/*z* calcd for $C_{78}H_{71}N_4O_6 + H^+$: 1161.55246 $[M + H]^+$; found: 1161.55264.

Computational method

DFT calculations were performed using the Gaussian 16 code.[35] The B3LYP functional[36] was used with a 6-311++G** basis set including diffuse and polarization orbitals. van der Waals dispersion forces were modelled *via* empirical dispersion corrections within the D3 scheme[37] of Grimme with the Becke–Johnson damping.[38] The polarizable continuum model[39] was employed to describe the chloroform solvent. XYZ files of the optimized structures are available as ESI.†

Conclusions

There are still some remaining challenges in the field of design of synthetic fluorescent probes for ACh. Here we have proved that it is possible to make fluorescent a HC by extending the conjugation of the CTV C_3-unit. The main advantages of such a strategy are the possibility to (1) introduce various fluorophores *via* the efficient and well-known Sonogashira reaction and (2) modify the size and the structure of the capsule without being limited by the presence of the fluorophore. The fluorescent HC binds the ACh with a 1 : 1 stoichiometry and an association constant similar to the one of fluorescent HCs already described. Nevertheless, if HCs usually bind ACh *via* cation π-interactions between the trimethyl ammonium sub-unit of the guest and the aromatic part of the CTV core, it is not the binding mode observed with the HC **1**. Here titration NMR experiments conducted with this HC show that the TREN unit is also able to interact with the quaternary ammonium and probably more strongly than the CTV bowl. Formation of such 1 : 1 ACh@HC **1** inclusion complexes is supported by DFT calculations, with a preference of about 20 kcal mol^{-1} for the one with the ammonium pointing towards the TREN part.

Notes and references

1 T. L. Mako, J. M. Racicot and M. Levine, *Chem. Rev.*, 2019, **119**, 322.

2 (*a*) E. V. Antina, E. V. Rumyantsev, N. A. Dudina, Y. S. Marfin and L. A. Antina, *Russ. J. Gen. Chem.*, 2016, **86**, 2209; (*b*) J. Zhang, F. Cheng, J. Li, J.-J. Zhu and Y. Lu, *Nano Today*, 2016, **11**, 309; (*c*) P. Alreja and N. Kaur, *RSC Adv.*, 2016, **6**, 23169; (*d*) L. Zhu, Z. Yuan, J. T. Simmons and K. Sreenath, *RSC Adv.*, 2014, **4**, 20398; (*e*) N. Kumar, V. Bhalla and M. Kumar, *Analyst*, 2014, **139**, 543; (*f*) I. Grabchev, D. Staneva and R. Betcheva, *Curr. Med. Chem.*, 2012, **19**, 4976; (*g*) L. Prodi, M. Montalti, N. Zaccheroni and L. S. Dolci, in *Topics in Fluorescence Spectroscopy: Advanced Concepts in Fluorescence Sensing Part A: Small Molecule Sensing*, ed. C. D. Geddes and J. R. Lakowicz, Springer US, Boston, MA, 2005, pp. 1–57.

3 (*a*) Q. Wang, H. Sheng, L. Jin, Z. Zhang, W. Wang and X. Tang, *Spectrochim. Acta, Part A*, 2019, **207**, 96; (*b*) A. Patil and S. Salunke-Gawali, *Inorg. Chim. Acta*, 2018, **482**, 99; (*c*) S. A. Rommel, D. Sorsche, M. Fleischmann and S. Rau, *Chem. – Eur. J.*, 2017, **23**, 18101; (*d*) K.-C. Chang, S.-S. Sun, M. O. Odago and A. J. Lees, *Coord. Chem. Rev.*, 2015, **284**, 111; (*e*) R. R. Chu, *Adv. Mater. Res.*, 2014, **1052**, 460; (*f*) A. Bencini, F. Bartoli, C. Caltagirone and V. Lippolis, *Dyes Pigm.*, 2014, **110**, 169; (*g*) H. T. Ngo, X. Liu and K. A. Jolliffe, *Chem. Soc. Rev.*, 2012, **41**, 4928; (*h*) R. M. Duke, E. B. Veale, F. M. Pfeffer, P. E. Kruger and T. Gunnlaugsson, *Chem. Soc. Rev.*, 2010, **39**, 3936.

4 (*a*) S. Suganya, S. Naha and S. Velmathi, *ChemistrySelect*, 2018, **3**, 7231; (*b*) L. You, D. Zha and E. V. Anslyn, *Chem. Rev.*, 2015, **115**, 7840; (*c*) E. Manandhar and K. J. Wallace, *Inorg. Chim. Acta*, 2012, **381**, 15.

5 W. Li, L. Wang, H. Tang and D. Cao, *Dyes Pigm.*, 2019, **162**, 934.

6 (*a*) E. Berni, L. Le Henaff, L. Jarrige, E. Girard, G. Jonusauskas, I. Gosse and S. Pinet, *Eur. J. Org. Chem.*, 2017, 3620; (*b*) H. Ahmad, B. W. Hazel, A. J. H. M. Meijer, J. A. Thomas and K. A. Wilkinson, *Chem. – Eur. J.*, 2013, **19**, 5081; (*c*) Y. Zhou, Z. Xu and J. Yoon, *Chem. Soc. Rev.*, 2011, **40**, 2222.

7 (*a*) J. Zielonka and B. Kalyanaraman, *Free Radical Biol. Med.*, 2018, **128**, 3; (*b*) Z. Xu and L. Xu, *Chem. Commun.*, 2016, **52**, 1094; (*c*) Y. Liu, Y. Hu, S. Lee, D. Lee and J. Yoon, *Bull. Korean Chem. Soc.*, 2016, **37**, 1661.

8 (*a*) K. Bera, A. K. Das, A. Rakshit, B. Sarkar, A. Rawat, B. K. Maity and S. Maiti, *ACS Chem. Neurosci.*, 2018, **9**, 469; (*b*) T. Pradhan, H. S. Jung, J. H. Jang, T. W. Kim, C. Kang and J. S. Kim, *Chem. Soc. Rev.*, 2014, **43**, 4684.

9 (*a*) Y. Xu, X. Wei, H. Li, X. Zheng, K. Lu, X. Liu, K. Wang and Y. Yan, *RSC Adv.*, 2016, **6**, 72715; (*b*) H. Jin, R. Gui, Z. Wang, F. Zhang, J. Xia, M. Yang, S. Bi and Y. Xia, *Analyst*, 2015, **140**, 2037.

10 (*a*) T. Tian, Y. He, Y. Ge and G. Song, *Sens. Actuators, B*, 2017, **240**, 1265; (*b*) X. Ren, J. Ge, X. Meng, X. Qiu, J. Ren and F. Tang, *Sci. Bull.*, 2016, **61**, 1615.

11 (*a*) Y. Feng, C. Dai, J. Lei, H. Ju and Y. Cheng, *Anal. Chem.*, 2016, **88**, 845; (*b*) H. Li, W. Kong, J. Liu, N. Liu, H. Huang, Y. Liu and Z. Kang, *Carbon*, 2015, **91**, 66.

12 (*a*) M. I. Halawa, F. Wu, T. H. Fereja, B. Lou and G. Xu, *Sens. Actuators, B*, 2018, **254**, 1017; (*b*) S. Govindaraju, S. R. Ankireddy, B. Viswanath, J. Kim and K. Yun, *Sci. Rep.*, 2017, **7**, 40298.

13 (*a*) C. Sun, F. Yuan, H. Li and X. Wu, *Microchim. Acta*, 2018, **185**, 317; (*b*) X. Ling, R. Shi, J. Zhang, D. Liu, M. Weng, C. Zhang, M. Lu, X. Xie, L. Huang and W. Huang, *ACS Sens.*, 2018, **3**, 1683; (*c*) S. Yang, X. Sun, Z. Wang, X. Wang, G. Guo and Q. Pu, *Sens. Actuators, B*, 2017, **253**, 752.

14 P. A. Rasheed and J.-S. Lee, *Microchim. Acta*, 2017, **184**, 1239.

15 (*a*) X. Zhang, Y. Zhu, X. Li, X. Guo, B. Zhang, X. Jia and B. Dai, *Anal. Chim. Acta*, 2016, **944**, 51; (*b*) K. S. Hettie and T. E. Glass, *ACS Chem. Neurosci.*, 2016, **7**, 21; (*c*) X. Zhu, X. Ge and C. Jiang, *J. Fluoresc.*, 2007, **17**, 655; (*d*) K. E. Secor and T. E. Glass, *Org. Lett.*, 2004, **6**, 3727.

16 J. Micheau and A. Marighetto, *Behav. Brain Res.*, 2011, **221**, 424.

17 L. M. Jordan, J. R. McVagh, B. R. Noga, A. M. Cabaj, H. Majczyński, U. Sławińska, J. Provencher, H. Leblond and S. Rossignol, *Front. Neural Circuits*, 2014, **8**, 132.

18 S. C. Dulawa and D. S. Janowsky, *Mol. Psychiatry*, 2019, **24**, 694.

19 (*a*) D. J. Selkoe, *Science*, 2002, **298**, 789; (*b*) G. Rizzi and K. R. Tan, *Front. Neural Circuits*, 2017, **11**, 110.

20 (*a*) H. Li, Y. Guo, L. Xiao and B. Chen, *Biosens. Bioelectron.*, 2014, **59**, 289; (*b*) Z. Chen, X. Ren, X. Meng, D. Chen, C. Yan, J. Ren, Y. Yuan and F. Tang, *Biosens. Bioelectron.*, 2011, **28**, 50.

21 (*a*) B. Hua, L. Shao, Z. Zhang, J. Sun and J. Yang, *Sens. Actuators, B*, 2018, **255**, 1430; (*b*) B. Bibal, *Supramol. Chem.*, 2018, **30**, 243; (*c*) A. Schena and K. Johnsson, *Angew. Chem., Int. Ed.*, 2014, **53**, 1302; (*d*) B. Mettra, Y. Bretonnière, J.-C. Mulatier, B. Bibal, B. Tinant, C. Aronica and J.-P. Dutasta, *Supramol. Chem.*, 2013, **25**, 672; (*e*) Y. Kubo, K. Tsuruzoe, S. Okuyama, R. Nishiyabu and T. Fujihara, *Chem. Commun.*, 2010, **46**, 3604; (*f*) N. Korbakov, P. Timmerman, N. Lidich, B. Urbach, A. Sa'ar and S. Yitzchaik, *Langmuir*, 2008, **24**, 2580.

22 (*a*) M.-L. Dumartin, C. Givelet, P. Meyrand, B. Bibal and I. Gosse, *Org. Biomol. Chem.*, 2009, **7**, 2725; (*b*) L. Peyrard, S. Chierici, S. Pinet, P. Batat, G. Jonusauskas, N. Pinaud, P. Meyrand and I. Gosse, *Org. Biomol. Chem.*, 2011, **9**, 8489.

23 D. Zhang, A. Martinez and J. P. Dutasta, *Chem. Rev.*, 2017, **117**, 4900.

24 A. Long, N. Fantozzi, S. Pinet, E. Genin, R. Pétuya, D. Bégué, V. Robert, J.-P. Dutasta, I. Gosse and A. Martinez, *Org. Biomol. Chem.*, 2019, **17**, 5253.

25 L. Peyrard, M.-L. Dumartin, S. Chierici, S. Pinet, G. Jonusauskas, P. Meyrand and I. Gosse, *J. Org. Chem.*, 2012, **77**, 7023.

26 C. D. Geddes, *Meas. Sci. Technol.*, 2001, **12**, R53.

27 L. Erieau-Peyrard, C. Coiffier, P. Bordat, D. Bégué, S. Chierici, S. Pinet, I. Gosse, I. Baraille and R. Brown, *Phys. Chem. Chem. Phys.*, 2015, **17**, 4168.

28 A. Schmitt, V. Robert, J.-P. Dutasta and A. Martinez, *Org. Lett.*, 2014, **16**, 2374.

29 Y. Makita, N. Katayama, H.-H. Lee, T. Abe, K. Sogawa, A. Nomoto, S.-I. Fujiwara and A. Ogawa, *Tetrahedron Lett.*, 2016, **57**, 5112.

30 A. Schmitt, B. Chatelet, S. Collin, J.-P. Dutasta and A. Martinez, *Chirality*, 2013, **25**, 475.

31 P. A. Frey, *Magn. Reson. Chem.*, 2001, **39**, S190.

32 C. Rapp, E. Goldberger, N. Tishbi and R. Kirshenbaum, *Proteins*, 2014, **82**, 1494.

33 A. M. Brouwer, *Pure Appl. Chem.*, 2011, **83**, 2213.

34 P. Gans, A. Sabatini and A. Vacca, HypSpec, 2008. http://www.hyperquad.co.uk.

35 M. J. Frisch, G. W. Trucks, H. B. Schlegel, G. E. Scuseria, M. A. Robb, J. R. Cheeseman, G. Scalmani, V. Barone, G. A. Petersson, X. Nakatsuji, H. Li, M. Caricato, A. V. Marenich, J. Bloino, B. G. Janesko, R. Gomperts, B. Mennucci, H. P. Hratchian, J. V. Ortiz, A. F. Izmaylov, J. L. Sonnenberg, D. Williams-Young, F. Ding, F. Lipparini, F. Egidi, J. Goings, B. Peng, A. Petrone, T. Henderson, D. Ranasinghe, V. G. Zakrzewski, J. Gao, N. Rega, G. Zheng, W. Liang, M. Hada, M. Ehara, K. Toyota, R. Fukuda, J. Hasegawa, M. Ishida, T. Nakajima, Y. Honda, O. Kitao, H. Nakai, T. Vreven, K. Throssell, J. A. Montgomery Jr, J. E. Peralta, F. Ogliaro, M. J. Bearpark, J. J. Heyd, E. N. Brothers, K. N. Kudin, V. N. Staroverov, T. A. Keith, R. Kobayashi, J. Normand, K. Raghavachari, A. P. Rendell, J. C. Burant, S. S. Iyengar, J. Tomasi, M. Cossi, J. M. Millam, M. Klene, C. Adamo, R. Cammi, J. W. Ochterski, R. L. Martin, K. Morokuma, O. Farkas, J. B. Foresman and D. J. Fox, Gaussian, Inc., Wallingford CT, 2016.

36 A. D. Becke, *J. Chem. Phys.*, 1993, **98**, 5648.

37 S. Grimme, J. Antony, S. Ehrlich and H. Krieg, *J. Chem. Phys.*, 2010, **132**, 154104.

38 S. Grimme, S. Ehrlich and L. Goerigk, *J. Comput. Chem.*, 2011, **32**, 1456.

39 G. Scalmani and M. J. Frisch, *J. Chem. Phys.*, 2010, **132**, 114110.